Improved limit on invisible decays of positronium

A. Badertscher,[1] P. Crivelli,[1] W. Fetscher,[1] U. Gendotti,[1] S. N. Gninenko,[2] V. Postoev,[2] A. Rubbia,[1] V. Samoylenko,[2] and D. Sillou[3]

[1]*ETH Zürich, Zürich, Switzerland*

[2]*Inst. Nucl. Research, INR Moscow, Russia*

[3]*Laboratoire Physique des Particules Annecy, LAPP, France*

(Received 9 October 2006; published 13 February 2007)

The results of a new search for positronium decays into invisible final states are reported. Convincing detection of this decay mode would be a strong evidence for new physics beyond the standard model (SM): for example, the existence of extra−dimensions, of milli-charged particles, of new light gauge bosons or of mirror particles. Mirror matter could be a relevant dark matter candidate. In this paper the setup and the results of a new experiment are presented. In a collected sample of about $(6.31 \pm 0.28) \times 10^6$ orthopositronium decays, no evidence for invisible decays in an energy [0,80] keV was found and an upper limit on the branching ratio of orthopositronium o-Ps $\rightarrow$ invisible could be set: Br(o-Ps $\rightarrow$ invisible) $< 4.2 \times 10^{-7}$(90%C.L.) Our results provide a limit on the photon mirror-photon mixing strength $\epsilon \leq 1.55 \times 10^{-7}$(90%C.L.) and rule out particles lighter than the electron mass with a fraction $Q_x \leq 3.4 \times 10^{-5}$ of the electron charge. Furthermore, upper limits on the branching ratios for the decay of parapositronium Br(p-Ps $\rightarrow$ invisible) $\leq 4.3 \times 10^{-7}$(90%C.L.) and the direct annihilation Br($e^+e^- \rightarrow$ invisible) $\leq 2.1 \times 10^{-8}$(90%C.L.) could be set.

DOI: 10.1103/PhysRevD.75.032004 PACS numbers: 13.40.−f, 13.40.Hq

I. INTRODUCTION

Although direct manifestations of new physics are searched for at the high energy frontier, new phenomena can also be looked for at low energies via precision measurements. The new effects might be observed in rare decays of the positronium (see e.g. [1]).

Positronium (Ps), the positron-electron bound state, is the lightest known atom, which at the current level of experimental and theoretical precision is bound and self-annihilates through the electromagnetic interaction [2]. This feature has made positronium an ideal system for testing the accuracy of quantum electrodynamics (QED) calculations for bound states, in particular, for the triplet (1^3S_1) state of Ps (orthopositronium, o-Ps) [3]. Because of the odd-parity under C-transformation o-Ps decays predominantly into three photons with a lifetime in vacuum of $\tau_{\text{o-Ps}} = 142.05$ ns [2–5]. The singlet (1^1S_0) state (parapositronium, p-Ps) decays predominantly into two photons with a lifetime in vacuum of $\tau_{\text{p-Ps}} = 125$ ps [6,7]. The longer lifetime of o-Ps (due to the phase-space and additional α suppression factors) gives an enhancement factor $\simeq 10^3$ in the sensitivity to an admixture of potential new interactions not accommodated in the standard model (SM) [8].

This paper focuses on a new search for o-Ps $\rightarrow$ invisible decays. By invisible we mean photonless decays, i.e. decays which are not accompanied by energy deposition in a hermetic calorimeter. In the SM the decay into a neutrino-antineutrino pair has a branching ratio of 6.6×10^{-18} [9]. Evidence for invisible decays in the region $\simeq 10^{-7}$ would, therefore, unambiguously signal the presence of new physics. New models that are relevant to the o-Ps $\rightarrow$ invisible decay mode predict the existence either of i) extra-dimensions [10,11], or ii) fractionally charged particles [12,13], or iii) a new light vector gauge boson [14], or iv) mirror particles, which could be candidates for dark matter [15–20].

The first experiment to search for invisible decay channels of o-Ps was performed by Atoyan *et al.* [21]. Their result on Br(o-Ps $\rightarrow$ invisible) $< 5.3 \times 10^{-4}$ (90% C.L.) excluded this channel as a possible explanation of the o-Ps lifetime anomaly (for a recent review, see e.g. [22]). This search was repeated by Mitsui *et al.* who found a branching ratio Br(o-Ps $\rightarrow$ invisible) $< 2.8 \times 10^{-6}$ (90% C.L.) [23]. Furthermore, they could place a limit on the existence of milli-charged particles and on the photon mirror-photon mixing. This result was corrected in [24] by taking into account the suppression factor for the mixing due to the presence of matter.

The rest of the paper is organized as follows. The details of the experimental setup are reported in Sec. II. The expected background is presented in Sec. III. In Secs. IV and V the data analysis and the results are described. The interpretation and the conclusion are reported in Secs. VI and VII.

II. EXPERIMENTAL TECHNIQUE AND SETUP

The experimental signature of o-Ps $\rightarrow$ invisible decays is the apparent disappearance of the energy $2m_e$ expected in ordinary decays in a hermetic calorimeter surrounding the o-Ps formation target. The readout trigger for the calorimeter is performed by tagging the stopping of a positron in the target with high efficiency.

 © 2007 The American Physical Society

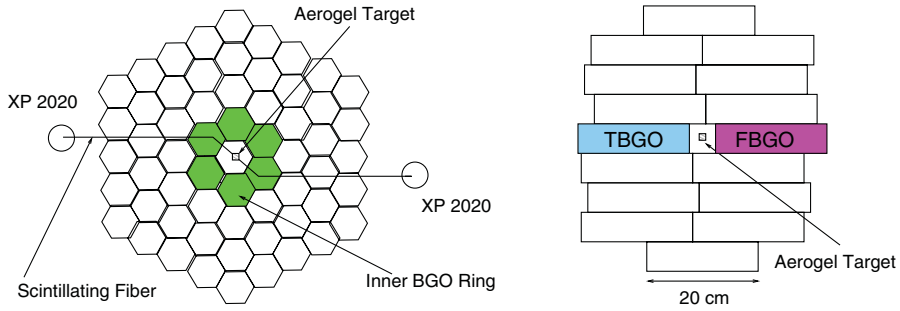

FIG. 1 (color). Schematic illustration of the experimental setup: a) front view, b) top view.

For the design of the experimental setup aiming at a sensitivity Br(o-Ps $\rightarrow$ invisible) $\simeq 10^{-8}$, the following criteria were considered:

(a) The probability not to detect all direct e^+e^- annihilation photons was suppressed to $\leq 10^{-9}$ using a thick hermetic crystal calorimeter, minimizing the dead material and with a good energy resolution. The probability to loose all photons in 3γ decays is consequently even smaller.

(b) The region around the target was designed with as little dead material as possible in order to reduce photon losses.

(c) By the appropriate choice of a porous target material and its dimensions a high fraction of o-Ps was produced resulting in a suppression of the background from the direct e^+e^- annihilation and p-Ps decays and in high statistics.

(d) The trigger rate and the DAQ speed were maximized for statistics.

(e) An efficient positron tagging system was designed to provide a clean trigger for positronium formation. A method was developed to suppress the background from the electrons emitted in the EC process (shake-off electrons).

(f) An efficient identification of the 1.27 MeV photon emitted by the ^{22}Na radioactive source was achieved with a method to veto the charged particles entering the trigger counter, thus, the backgrounds related to them could be reduced.

The schematic illustration of the detector setup is shown in Fig. 1 (the detailed description of the experimental technique and setup can be found in Refs. [25,26]).

Positrons are produced from a ^{22}Na source with an activity of $\simeq 30$ kBq. The ^{22}Na has a half life of 2.6 yr and has a Q-value for the nuclear transition to ^{22}Ne of $Q = 2.842$ MeV. This is the maximum energy available for the particles involved in one of the three possible decay modes of ^{22}Na:

(A) Decay mode A (Br $\simeq 90.6\%$): the β^+ decay with endpoint energy 0.546 MeV. The positron is always followed by the prompt emission of a 1.27 MeV photon ($\tau \simeq 3.7$ ps) from the ^{22}Ne* de-excitation to the ground state.

(B) Decay mode B (Br $\simeq 9.44\%$): the Electron Capture process (EC), where an orbital electron is captured by the nucleus, and only a 1.27 MeV photon and a neutrino are emitted from the source. In some rare cases (with a probability $\simeq 6 \times 10^{-3}$), an orbital electron is ejected, due to the sudden change in the nucleus charge (shake-off) [27].

(C) Decay mode C (Br $\simeq 0.056\%$): there is no photon emission because the transition goes directly to the ground state. The endpoint energy of the positron is 1.83 MeV.

Therefore, in most o-Ps (p-Ps) decays we expect 3(2) photons with a summed energy equal to $2m_e$ and one photon with an energy of 1.27 MeV (see Fig. 2).

Photons from the direct e^+e^- annihilation in flight or from the positronium decays were detected in a hermetic, segmented BGO calorimeter (the ECAL). Two endcap counters called TBGO and FBGO (see Figs. 1 and 2) surrounded the target on each side. At the analysis level the 1.27 MeV photon (“the triggering photon”) was required to be identified in the TBGO counter. The calorimeter was instrumented with charge and time readout.

The activity of the source was chosen to maximize the trigger rate versus the inefficiency of signal detection (mostly due to pileup events). The source was prepared by evaporating drops of a ^{22}Na solution directly on a 100 μm thick and 2×8 mm^2 wide plastic scintillator

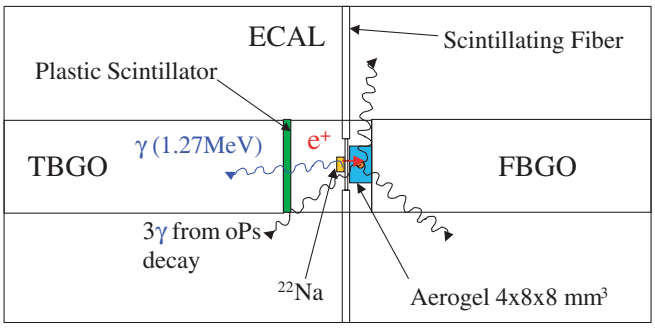

FIG. 2 (color). Schematic illustration of the positron tagging system and the o-Ps formation target of the setup.

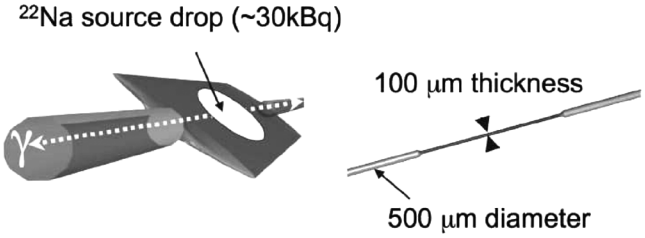

FIG. 3. Schematic view of the scintillating fiber with the ^{22}Na source on the squeezed part in the center.

(see Fig. 3) fabricated by squeezing a 500 μm diameter scintillating fiber (Bicron BF-12). In this way, no dead material was introduced for a source holder. The S-shape of the fiber (see Fig. 1) was selected to avoid background from back-to-back 511 keV annihilation photons. The scintillating fiber was read out at both ends by two photomultipliers (Philips XP2020) located outside the detector (see Fig. 1). The coincidence of the two PMT signals was used to tag the passage of a positron through the fiber and acted as a start signal for the data readout system. The use of two PMTs in coincidence, instead of a single one [23], lowered the ratio between fake and real positron triggers to $<1.9 \times 10^{-10}$.

Opposite to the source, a $4 \times 8 \times 8$ mm^3 SiO_2 aerogel piece (type SP30, purchased from Matsushita Electric Works) was placed in contact with the squeezed fiber (see Fig. 2 and 4). Positrons stopping in the aerogel target may form positronium (the formation probability is 45% [28]) which can migrate into the aerogel pores. The collisions with the walls of the pores did not appreciably quench the o-Ps: when the aerogel was flushed with nitrogen, a fit to the distribution of the time difference between the start from the fiber and the stop from the calorimeter yielded $\tau_{\text{o-Ps}} = 128.1 \pm 1.8$ ns, which is very close to the lifetime in vacuum $\tau_{\text{o-Ps}} \simeq 142.05 \pm 0.02$ ns [29].

The ECAL was composed of 100 BGO crystals that surrounded the target region providing a nearly isotropic

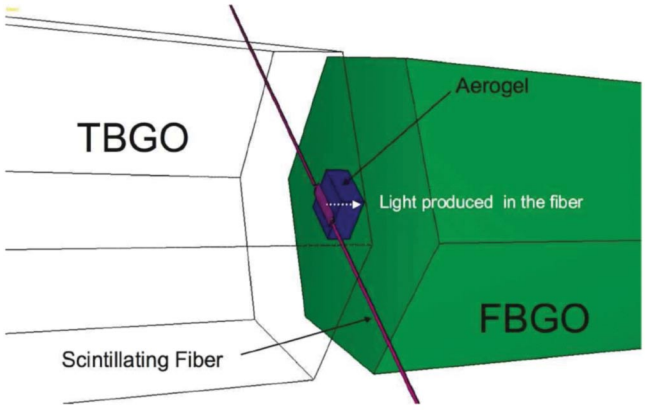

FIG. 4 (color). Schematic illustration of the method to readout the energy deposition in the fiber.

sphere of radius 200–220 mm (see Fig. 1). Each crystal had a hexagonal cross section of 61 mm diameter and a length of 200 mm. The crystals of the inner most ring were wrapped in a 2 μm thick aluminized Mylar foil to minimize the photon energy absorption. The other crystals were wrapped with Teflon foils of 750 μm thickness. The crystals in the barrel and the FBGO were readout with ETL 9954 photomultiplier tubes.

The energy deposited in the fiber is an important parameter in order to reject the background from the electrons emitted in the EC process (shake-off electrons, see Sec. III). The mean number of photoelectrons detected in each XP2020 for a positron crossing the fiber was measured to be about 1.2, thus, a cut on the energy deposited in the fiber using these signals would not be meaningful. For this reason the FBGO was also used to measure the energy deposited in the fiber by the positron: the light emitted by the fiber could traverse the transparent aerogel and enter the FBGO through an aperture in the wrapping on its front face. This light was then guided by the FBGO to the PMT attached on the back face of FBGO (as illustrated in Fig. 4). This method provided a mean number of photoelectrons equal to 13 ± 1 for a positron traversing the fiber [26].

The TBGO signal was used in the offline analysis to identify the 1.27 MeV photon. The energy resolution of the TBGO was an essential parameter to reduce backgrounds related to the misidentification of the 1.27 MeV photon (see also Sec. III). To provide a better energy resolution, this crystal was coupled to an ETL 9964 PMT with a more uniform light collection and a larger quantum efficiency than the ETL 9954. For the same reason this crystal was of a better quality than the others and efforts were dedicated to maximize the light collection by keeping the amount of dead material introduced by the crystal wrapping as small as possible. The best results were achieved with the crystal wrapped in the 3M radiant mirror (64 μm thickness): the resolution at 662 keV was measured to be about 15% (FWHM). To select the triggering photon, an energy $[1275 \pm 67]$ keV was used in the analysis. In addition, to veto charged particles (positrons and electrons) entering the TBGO, a 1 mm thick plastic scintillator (Bicron BC-400) was optically coupled to the TBGO front face (for more details see [30]), i.e. the same PMT was used to detect the light signals from the plastic scintillator and the TBGO crystal (see Sec. III for a discussion of backgrounds associated to charged particles entering the TBGO). For both, TBGO and FBGO counters the signals from the plastic scintillator or from the fiber could be distinguished from the signal of the BGO crystal due to their significantly different decay times, e.g. $\tau \simeq 2.7$ ns for plastic scintillator and $\tau \simeq 300$ ns for BGO. To carry out the measurements the outputs of these counters were passively split into three signals which were fed into corresponding ADC inputs with three different integration gates, as illustrated in Fig. 5. The first one, the normal long gate was used to

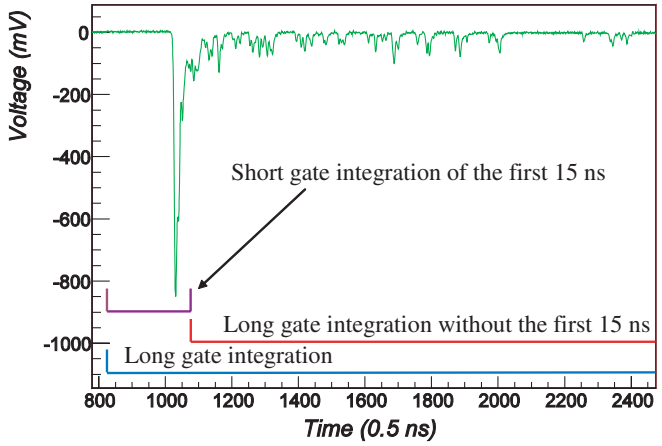

FIG. 5 (color online). An example of the pulse shape of the FBGO signal which is an overlap of signals from a positron and a photon, detected in the fiber and BGO crystal, respectively. The short gate was used to measure the energy loss from positrons (shown not in scale). See text for the detailed description of the used gates.

measure the full energy deposition in the counter, i.e. the sum of energies deposited in the crystal and scintillator. The second, a short gate, was used to measure the energy loss in the plastic scintillator or in the fiber, and the third one, a gate delayed with respect to the trigger long gate, was used to measure the pure photon energy deposited in the FBGO counter and for better identification of the 1.275 MeV trigger photon in TBGO, respectively.

The light signal corresponding to energy deposition from a positron crossing the fiber could, in principle, contaminate through the entrance the energy from o-Ps decay or veto information in the FBGO counter, i.e. could be taken as a energy deposition from the original positron annihilation. To study this effect, clean samples of events corresponding to detection of two 511 keV annihilation photons in any of two back-to-back BGO counters surrounding the FBGO crystal were selected. For this sample only the fiber light could give a signal in FBGO, since the, so-called, optical cross-talk was much less than 1%. The FBGO pedestal, its width, and the response to 511 keV photons were measured as a function of the long gate delay and compared for two cases—the entrance closed and open, i.e. with and without screening of the fiber light.

Finally, the delay of 15 ns was chosen to compromise the reduction of the number of detected photoelectrons in the FBGO counter and the broadening of its pedestal. The pedestal width (FWHM) measured with and without screening the fiber light changes from 17 to 20 keV, respectively. The increase was due to contributions from the fiber light tail and possibly from the fiber afterglow. This broadening was small compared to the FWHM of the sum of all pedestals (FWHM $\simeq$ 80 keV) used in the analysis and results in a negligible contribution to the o-Ps $\rightarrow$ invisible signal efficiency loss, which was dominated by the overlap of close in time events (see below).

In Fig. 6 the scatter plot of signals measured with short versus long gate is shown for the TBGO counter coupled with the front face to the plastic scintillator. Three regions corresponding to detection of a) pure positrons stopped in the plastic scintillator, b) 511 keV photons contaminated by the positron energy deposited in scintillator, and c) pure photons, i.e. without detection of positrons in the plastic scintillator are clearly seen. The ellipse indicates the one sigma contour of the 1.275 MeV peak with a barely visible tail from positrons detected in the plastic scintillator. In order to avoid reduction of the statistics and due to the typically high pulse height from the positron energy, it was found possible to use instead of a charged particle veto cut on the energy loss measured with the short gate, an energy cut around the 1.275 MeV photopeak. Thus, this single cut results in the charged veto to suppress positrons entering the TBGO and in the 1.27 MeV trigger photon identification with a purity found to be better than 90%. A remaining $\simeq$ 10% of events contaminated by positron energy are not dangerous, because they correspond to positrons stopped in the plastic scintillator and not entering the crystal. Finally, this cut was enhanced by adding a cut on the energy deposition in the delayed long gate, see Fig. 7(f) and 7(g) below, resulting in a slightly improved purity of trigger photon events.

A VME system interfaced to a PC was used for data acquisition (the DAQ rate was about 1800 events/s). For every trigger, five CAEN QDCs v792 modules (32 chan-

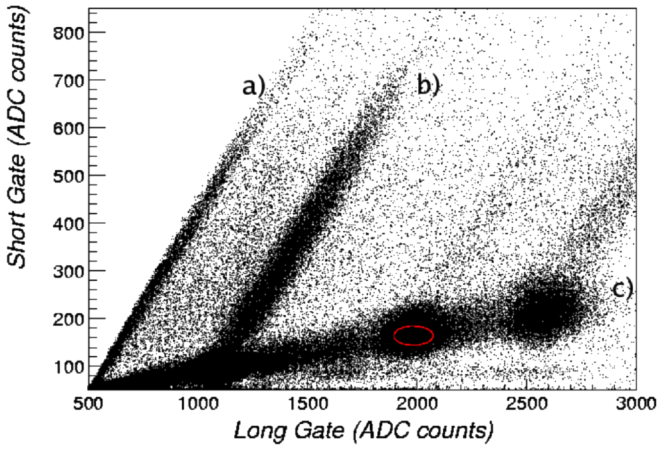

FIG. 6 (color online). The scatter plot of energy loss measured with the short versus long gate for the TBGO counter coupled with the front face to the plastic scintillator. Three regions corresponding to detection of a) pure positrons detected in the plastic scintillator, b) 511 keV photons contaminated by the positron energy deposited in scintillator, and c) pure photons, i.e. without detection of positrons in the plastic scintillator are clearly seen. The ellipse indicates the one sigma contour of the 1.275 MeV peak with a barely visible tail from positrons detected in the plastic scintillator.

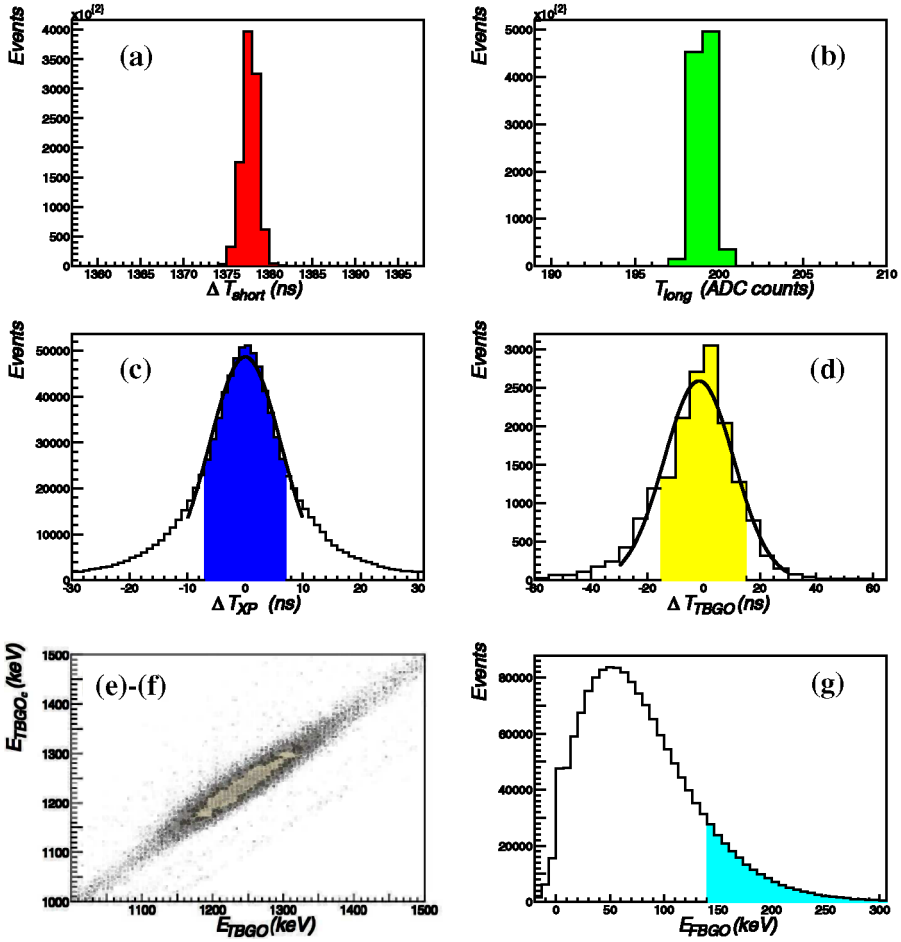

FIG. 7 (color online). The cuts applied to the variables. The numbers on the plot correspond to the variable defined in the text (Sec. IV). Only the colored regions contribute to the signal.

nels) recorded the charge of the crystal signals while a CAEN TDC v775 recorded the time information. A trigger gate length of 2.9 μs was chosen to keep the probability of o-Ps to decay after this time to $\lesssim 10^{-9}$.

A temperature stabilized light-tight box containing the calorimeter was built in order to keep the temperature variation of the BGO crystals in the range of $\pm 0.5\,^{\circ}$C. Water, whose temperature was controlled by two thermostats, circulated through copper tubes welded on two copper plates inside the box. The experimental hall was air conditioned to keep temperature variations within $\pm 1\,^{\circ}$C. The high-voltage dividers of all PMTs were placed outside the box in order to avoid energy dissipation close to the crystals. The BGO crystals were equipped with LEDs that could be pulsed periodically to monitor the response. Additionally, the gains of the PMTs were also monitored to check their stability.

The detector was calibrated and monitored internally using the 511 keV annihilation photon and the 1.27 MeV photons emitted by the ^{22}Na source. Variations of the energy scale during the run period were within $\lesssim 1\%$ and corrected on the basis of an internal calibration procedure [26].

III. BACKGROUND ESTIMATION AND DEDICATED ENGINEERING RUN

In order to reach the required sensitivity, the background had to be reduced and controlled at the level of 10^{-8}. To understand the different background sources and to cross-check the simulation, we performed an engineering run with a simplified version of our detector. During two months of data taking, the stability of the detector and its components was investigated. The comparison between the background expected from Monte Carlo (MC) simulations and the data of the engineering run is summarized in Table I.

The ECAL thickness of 200 mm provides a probability of $<10^{-9}$ for two 511 keV photons to escape detection (see background 1 in Table I). For three-photon decays, this probability is consequently even smaller.

If one (or more) annihilation photon (e.g. backscattered from the target) overlaps with the 1.27 MeV in the TBGO, it can fall in the trigger energy $[1275 \pm 67]$ keV because of the finite energy resolution. This introduces a background if the remaining annihilation photon gets absorbed in the dead material or escapes detection. The separation between

TABLE I. Comparison between expected and measured background level for the different background sources in the engineering run and expected background level for the final setup (see text for details).

BACKGROUND SOURCE		ENGINEERING RUN		FINAL SETUP
		expected	measured	expected
1)	Hermiticity Dead Material Resolution	$<10^{-9}$	$<10^{-9}$	$<10^{-9}$
2)	Absorption in trigger Energy window	1.3×10^{-6}	1.5×10^{-6}	$<5 \times 10^{-9}$
3)	MS positron with $E_{\max} = 546$ keV	2.1×10^{-6}		$<10^{-8}$
4)	MS positron with $E_{\max} = 1.83$ MeV	1.4×10^{-7}		$<10^{-8}$
5)	Compton EC photon	1.3×10^{-6}		$<10^{-8}$
6)	Accidental noise and EC photon	3.2×10^{-11}	$<1.9 \times 10^{-10}$	1.9×10^{-10}
7)	Shake-off electrons in EC process	10^{-6}–10^{-7}		10^{-8}
Total		4.8×10^{-6}	5.6×10^{-6}	10^{-8}

the upper bound of the trigger energy and the sum of a triggering and a 511 keV photon was, thanks to the good energy resolution of the TBGO, 7σ of the 1786 keV peak (1275 + 511 keV). Thus, the level of this background is $<5 \times 10^{-9}$ (background 2 in Table I).

In order to suppress the other sources of background related to the misidentification of the 1.27 MeV photon (backgrounds 3, 4 and 5 listed in Table I), one had to veto charged particles entering the TBGO. Two processes are responsible for generating such triggers. One is associated with decay mode B (EC) when the 1.27 MeV photon interacts in the fiber, faking a positron signal. If the scattered photon and the Compton electron reach the TBGO, the sum of the energy of the two particles can be misidentified as the triggering photon without any energy in the rest of the calorimeter. Another background can occur in decay mode A if the 1.27 MeV photon is not detected: a trigger can be produced by a positron that multiple scatters (MS) in the fiber and deposits enough energy to trigger the experiment. If the positron reaches the TBGO with a kinetic energy of about 200–300 keV and the two 511 keV annihilation photons are completely absorbed in the TBGO an energy close to 1.27 MeV will be reconstructed. This will appear as an invisible decay since no energy is expected in the rest of the detector. If the 1.27 MeV photon is not present (decay mode C) a trigger can similarly be produced by the 1.83 MeV positron. To veto these backgrounds the energy cut of the TBGO signal described in the previous section was used such that the backgrounds 3, 4 and 5 had a probability of $<10^{-8}$ in the final setup.

The EC photon may accidentally coincide with a trigger from the fiber generated either by the PMTs noise or by some other particles emitted from possible unstable isotopes formed during the target activation. The level of this background could be reduced with the selection of two XP 2020 with very low noise (< 30 counts/s) and the requirement of the coincidence between them. In addition, a radioactive source with a controlled high purity was chosen. From the data of the engineering run, this background was estimated to be $<1.9 \times 10^{-10}$ (background 6 in Table I).

During the decay mode B (EC) the fiber signal can be generated by shake-off electrons (background 7 in Table I). Since the probability of an electron ejection steeply drops with its emission kinetic energy (more than 4 orders of magnitude in the first 100 keV) the cut on the energy deposited in the fiber by the triggering particles was used to suppress this background.

The engineering run allowed to test these backgrounds as shown in Table I. The expected fraction of zero energy events is 10% smaller than what was measured. This difference can be explained by the contribution from the shake-off electrons which was not included in the simulation. Indeed, in the engineering run there was no information about the energy deposited in the fiber so that no cut on the energy of the particles passing through the fiber could be applied.

The last column of the table lists the expectations for the final setup. The total background is estimated to be at the level 10^{-8}. The threshold on the energy deposited in the fiber was set considering the uncertainty due to the number of photoelectrons and the subtraction method to be sure that no electron below 100 keV could trigger the fiber; it was chosen, based on simulations, to be at 140 keV.

IV. DATA ANALYSIS

For the analysis we used a data sample of 1.39×10^{10} recorded fiber triggers collected over a four months data taking period. For each event the following variables were used and cuts were applied to suppress background:

(1) ΔT_{short} is the time from the trigger start to the end marker of the dual timer unit that generates the short gate (measuring the light from the plastic scintillator coupled to the TBGO).
(2) ΔT_{long} is the pedestal of one of the QDC channels integrated using the long gate as a start trigger.
(3) ΔT_{XP} is the time difference between the two XPs reading the fiber.

(4) ΔT_{TBGO} is the time difference between the XPs coincidence and the TBGO.
(5) E_{TBGOc} is the energy deposited in the TBGO with a gate delayed by 15 ns to measure the energy deposited in the TBGO crystal without the contribution of the plastic scintillator.
(6) E_{TBGO} is the energy deposited in the TBGO with the full gate (long gate).
(7) E_{FBGO} is the energy deposition in the fiber measured with the FBGO.

The distributions of these variables for a reduced data sample of 10^6 triggers are shown in Fig. 7. The used selection cuts are listed in Table II. The cuts were selected and tuned with the help of a dedicated run with statistics corresponding to about 5% of the data. These variables can be grouped in three categories, depending on their function: (a) The first two variables check the stability of the electronics and the duration of the gate widths. The selection has been tuned experimentally looking at the obtained spectra. (b) The variables 3) and 4) suppress accidental triggers faking positrons in the fiber. The cuts have been chosen to minimize the accidentals and maximize the signal statistics. (c) The variables 5) to 7) are the cuts that reduce triggers from backgrounds that mimic the appearance of a positron in the formation cavity region. Furthermore, the upper limit of the energy for the 1.27 MeV photon is very sensitive to the background from the ''absorption'' of one 511 keV γ in the trigger energy window. The cut of $\pm 1\sigma$ was selected in order to enhance good triggers to the required level.

All the selection cuts, except 7), have been defined in terms of the sigma of the signal determined with a Gaussian fit to the data sample with 10^6 events. Table II summarizes the values used and the evolution of the total number of events passing the cuts.

The lower cut for the energy deposited in the fiber has been chosen to reduce the probability of shake-off electrons to trigger the fiber to a level $<10^{-8}$ as discussed in Sec. III. The measured fraction of the o-Ps produced in the aerogel is reduced by 20% applying the threshold for the energy cut in the fiber. This was expected, since the positrons that deposit the most energy are the ones stopping in the fiber.

V. RESULTS

After imposing the above requirements a final sample of 1.41×10^8 events was obtained. For these events the energies of all the 100 BGO crystals, except the TBGO, were summed. Figure 8 shows the spectrum of the total energy (E_{tot}) deposited in the ECAL. The peak at 1022 keV corresponds to the positronium mass ($M_{Ps} \simeq 2m_e$). The inset shows an extrapolation to the zero energy region.

To define the upper energy cut on E_{tot}, below which an event is considered as photonless (invisible), a dedicated run of 10^7 triggers was performed triggering the experiment only with the 1.27 MeV photon and no requirement of the fiber signal [21]. The zero peak contained about $10.4 \pm 1.2\%$ of the events passing the selection cuts defined in Sec. IV. This value was corrected by the inefficiency of zero signal detection and by a factor 0.8 determined using the MC simulations to take into account the different detection efficiencies of the 1.27 MeV photon in the case of the EC process and in the case of the transition with the positron. The measured value was consistent with the expected fraction of electron capture events (decay mode B). The cut $E_{\mathrm{tot}} < 80$ keV corresponding to the region containing 87% of the events in the EC peak at zero energy was used to define the photonless events, as shown in Fig. 9.

To determine the signal inefficiency, mostly due to pileup, $\simeq 10^6$ events have been collected using a random trigger formed by delaying the fiber coincidence by 16 μs (half of the mean time interval between two events). For the 80 keV threshold defined above, this gave an inefficiency of $(11.6 \pm 0.5)\%$ that was consistent with the prediction of the simulation. This inefficiency was measured at the beginning of the data taking and, conservatively, was not corrected for the reduction of the source intensity during that period. Finally, the signal efficiency was estimated to be $\epsilon \simeq (87.4 \pm 0.5)\%$.

The mean fraction of o-Ps in the data sample could be evaluated from the decay time curve by fitting the observed

TABLE II. Definition of cuts and the remaining fraction of events after the cut is applied.

Variable name	Selection cut		Fraction of events remaining after cuts
	# σ's	value of 1σ	
1) $\Delta T_{\mathrm{short}}$	$\pm 4\sigma$	1.03 ns	99.3%
2) ΔT_{long}	$\pm 4\sigma$	0.8 ADC counts	98.9%
3) ΔT_{XP}	$\pm 1\sigma$	1.87 ns	75.5%
4) ΔT_{TBGO}	$\pm 1\sigma$	3.71 ns	27.2%
5) E_{TBGO}	$\pm 1\sigma$	74 keV	3.1%
6) E_{TBGOc}	$\pm 1\sigma$	67 keV	2.7%
7) E_{FBGO}	140 keV $< E_{\mathrm{FBGO}} <$ 400 keV		1.1%

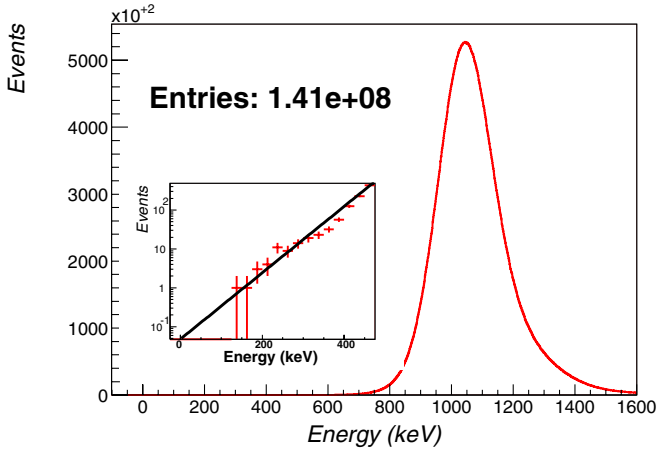

FIG. 8 (color online). Spectrum of the sum of the total energy in the ECAL. The inset shows the magnified view of the low-energy region in logarithmic scale. The signal range for the o-Ps → invisible decay is shown in Fig. 9.

distribution to the function $A \cdot e^{(-t/\tau_{\text{o-Ps}})} + B$ (B is the accidental background) starting from the time t = 100 ns when o-Ps was completely thermalized in the target, as shown in Fig. 10 [26]. After taking into account the estimated difference of efficiencies for 2 and 3 gamma detection and the pick-off effect (measured from the lifetime spectra with the same method as described in Ref. [31]), the fraction of o-Ps in the data sample obtained with the cut on E_{FBGO} (see Table II) was 4.5 ± 0.2% [26].

Since in the signal region no zero energy events were observed, the upper limit for the branching ratio [29] is

$$\text{Br(o-Ps} \rightarrow \text{invisible)} = 2.3/(N_{\text{o-Ps}} \cdot \epsilon) \leq 4.2 \times 10^{-7}(90\%\text{C.L.}) \quad (1)$$

where $N_{\text{o-Ps}} = (6.31 \pm 0.28) \times 10^6$ is the number of o-Ps in the selected sample. Figure 8 shows the extrapolation

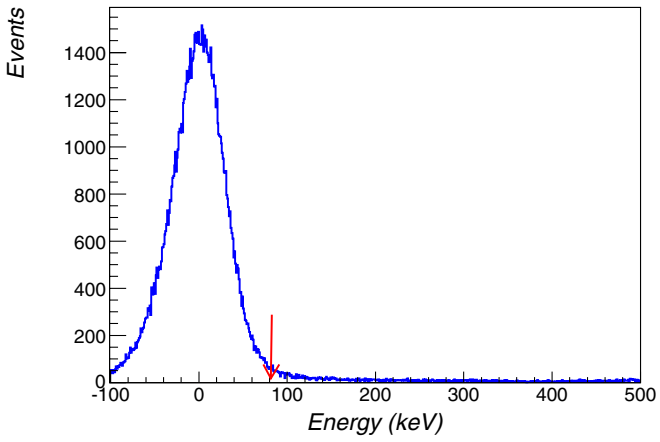

FIG. 9 (color online). Distribution of the sum of pedestals of all ECAL counters. The arrow indicates the threshold of 80 keV used to define the signal range for the o-Ps → invisible decay.

into the region of the zero signal with an exponential. The integral over this region gives an evaluation of the background contribution $N_{\text{bkg}} = 0.34 \pm 0.04$ of expected events, where the error was evaluated from the uncertainty related to the extrapolation procedure itself.

This experiment can also be used to obtain upper limits on Br(p-Ps → invisible) and on Br(e^+e^- → invisible). For this purpose the different probabilities of positrons stopping in the fiber and in the aerogel were calculated with the help of simulations. Several papers were reviewed in Ref. [23] concluding that the probability to form positronium (75% of o-Ps and 25% of p-Ps) per positron stopping is about 0.45 in the aerogel and between 0.2 and 0.4 in the fiber. In the aerogel a fraction of 0.05 to 0.1 of the p-Ps atoms experience pick-off annihilation in about 2 ns before escaping out of the silica grains in the pores. For o-Ps this probability ranges from 0.28 to 0.45. In a plastic scintillator (the fiber) the corresponding pick-off probabilities are 0.99 to 1 for o-Ps and 0.05 to 0.1 for p-Ps [23]. From the simulations, the fraction of positrons stopping in the fiber is 0.43 and in the aerogel is 0.25, therefore, the smallest possible fraction of p-Ps decays (including pick-off) is 5.5%. Thus, an upper bound for the invisible decay of p-Ps can be calculated

$$\text{Br(p-Ps} \rightarrow \text{invisible)} = 2.3/(N_{\text{p-Ps}} \cdot \epsilon) \leq 4.3 \times 10^{-7}(90\%\text{C.L.}) \quad (2)$$

where $N_{\text{p-Ps}} = 0.055 \times 1.41 \times 10^8 \simeq 6.14 \times 10^6$ was used and the positrons that do not stop in the fiber or in the aerogel are assumed to annihilate directly. The number of e^+e^- decays can be calculated subtracting from the total number of events the p-Ps and o-Ps decays, thus, one obtains $N_{e^+e^-} \simeq 1.29 \times 10^8$ and an upper limit for the branching ratio of

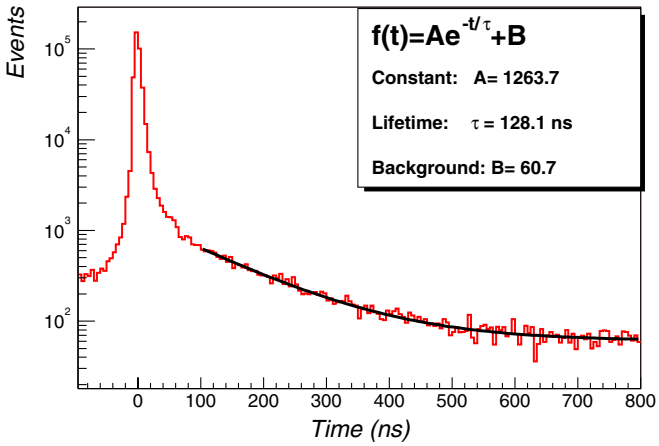

FIG. 10 (color online). Distribution of the time between the fiber trigger and one of the annihilation photons in the TBGO. The curve shows the fit to the function $A \cdot e^{(-t/\text{o-Ps})} + B$ starting from 100 ns when the o-Ps is completely thermalized in the target.

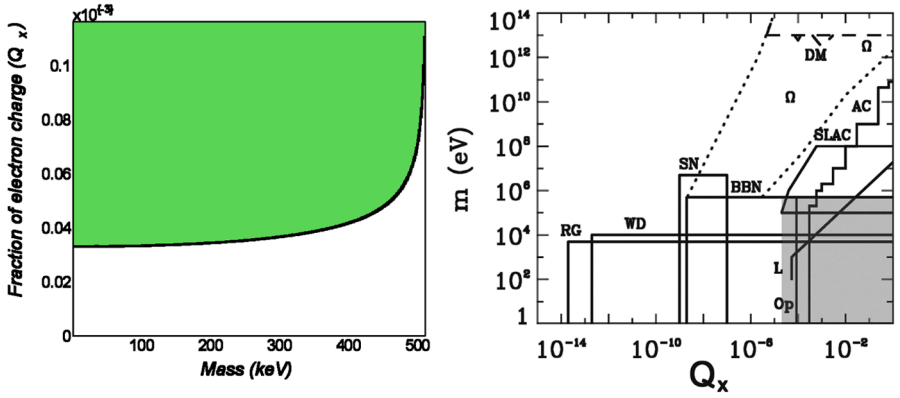

FIG. 11 (color online). a) Mass-charge parameter space for the o-Ps decay into milli-charged particles, excluded with this experiment, b) Comparison of our results (the dashed region on the plot) with other experimental (SLAC [32] and previous o − Ps → invisible [23]) and astrophysical bounds (the plot was taken from [13]).

$$\mathrm{Br}(e^+e^- \to \text{invisible}) = 2.3/(N_{e^+e^-} \cdot \epsilon) \leq 2.1 \times 10^{-8}(90\%\text{C.L.}) \quad (3)$$

VI. INTERPRETATION

No event consistent with an invisible decay was found in the large sample of events.

Using Eq. (32) of Ref. [14], the bound for particles with a fraction Q_x of the electron charge can be plotted as a function of their mass m_X for $m_X < m_e$, as shown in Fig. 11(a). Thus, the region of the charge-mass parameter space, which was not excluded directly by the SLAC results [32] and the previous search for o-Ps → invisible [23], is covered by this experiment [see Fig. 11(b)].

The strength of the photon mirror-photon mixing ϵ can be extracted from the limit on the Br(o-Ps → invisible) with [24]

$$\epsilon = \frac{1}{2\pi f}\sqrt{\frac{\mathrm{Br}(\text{o-Ps} \to \text{invisible})\Gamma_{\mathrm{SM}}\Gamma_{\mathrm{coll}}}{2(1 - \mathrm{Br}(\text{o-Ps} \to \text{invisible}))}} \quad (4)$$

by substituting a conservative value of $\Gamma_{\mathrm{coll}} = 5 \times 10^4\ \mathrm{s}^{-1}$ for the collision rate of the o-Ps against the walls of the aerogel pores [17]. Γ_{SM} is the decay rate of o-Ps in vacuum and $f = 8.7 \times 10^4$ MHz is the contribution to the ortho-para splitting from the one-photon annihilation diagram involving o-Ps [16]. Using our result one can estimate the mixing strength to be $\epsilon \leq 1.55 \times 10^{-7}(90\%\text{C.L.})$. This is close to the BBN limit of $\epsilon < 3 \times 10^{-8}$ [33] but does not cover all the region of interest suggested by the DAMA and CRESST results [34] and motivated by GUT predictions [18] and by string theory [35] ($\epsilon > 10^{-9}$).

VII. CONCLUSION

In this paper the results of a new search for an invisible decay of o-Ps were reported. Since no event was found in the signal region, an upper limit for the branching ratio was set

$$\mathrm{Br}\,(\text{o-Ps} \to \text{invisible}) \leq 4.2 \times 10^{-7}(90\%\text{C.L.}) \quad (5)$$

improving the best existing bound [23] by a factor 7.

Analyzed in the context of theoretical models the negative result provides an upper limit on the photon mirror-photon mixing strength $\epsilon \leq 1.55 \times 10^{-7}(90\%\text{C.L.})$ and rules out particles with a fraction $Q_x \leq 3.4 \times 10^{-5}$ (for $m_X \leq m_e$) of the electron charge (milli-charged particles). Furthermore, an upper limit on the branching ratios for the process Br(p-Ps → invisible) $\leq 4.3 \times 10^{-7}(90\%\text{C.L.})$ and $\mathrm{Br}(e^+e^- \to \text{invisible}) \leq 2.1 \times 10^{-8}(90\%\text{C.L.})$ could be set.

ACKNOWLEDGMENTS

We thank the Paul Scherrer Institute (Villigen, Switzerland) for lending us the BGO crystals. We gratefully acknowledge the help of B. Eichler and J. Neuhausen for the ^{22}Na source preparation. We wish to thank Z. Berezhiani, R. Eichler, S. Karshenboim, N. V. Krasnikov, V. A. Matveev and V. A. Rubakov for useful discussions. We are grateful to N. A. Golubev, L. Knecht, G. Natterer, J. P. Peigneux and M. Sauter for their essential help. We wish to thank M. Haguenauer for providing us with samples of scintillating fibers. This work was supported by the Swiss National Science Foundation, by the INR Moscow, and by the French Ministery of Foreign Affairs through an ECONET program. We thank the CERN for its hospitality.

[1] *Proceedings of the Workshop on Positronium Physics*, edited by M. Felcini, S. N. Gninenko, A. Nyffeler, and A. Rubbia [Int. J. Mod. Phys. A 19, No. 23 (2004)].

[2] G. S. Adkins, R. N. Fell, and J. R. Sapirstein, Ann. Phys. (N.Y.) **295**, 136 (2002).

[3] S. Karshenboim, Int. J. Mod. Phys. A **19**, 3879 (2004).

[4] R. S. Vallery, D. W. Gidley, and P. W. Zitzewitz, Phys. Rev. Lett. **90**, 203402 (2003).

[5] O. Jinnouchi, S. Asai, and T. Kobayashi, Int. J. Mod. Phys. A **19**, 3927 (2004).

[6] A. Czarnecki, K. Melnikov, and A. Yelkhowsky, Phys. Rev. Lett. **83**, 1135 (1999).

[7] A. H. Al-Ramadhan and D. W. Gidley, Phys. Rev. Lett. **72**, 1632 (1994).

[8] S. N. Gninenko, N. V. Krasnikov, V. A. Matveev, and A. Rubbia, Phys. Part. Nucl. **37**, 321 (2006).

[9] A. Czarnecki and S. Karshenboim, *Proceedings of the 14th International Workshop on High Energy Physics and Quantum Field Theory (QFTHEP 99), Moscow, 1999*, edited by B. B. Levchenko and V. I. Savrin (MSU-Press, Moscow, Russia, 2000), pp. 538–544; J. Govaerts and M. Van Caille, Phys. Lett. B **381**, 451 (1996).

[10] S. L. Dubovsky, V. A. Rubakov, and P. G. Tinyakov, Phys. Rev. D **62**, 105011 (2000).

[11] S. N. Gninenko, N. V. Krasnikov, and A. Rubbia, Phys. Rev. D **67**, 075012 (2003).

[12] B. Holdom, Phys. Lett. **166B**, 196 (1986).

[13] S. Davidson *et al.*, J. High Energy Phys. 02 (2002) 37.

[14] S. N. Gninenko, N. V. Krasnikov, and A. Rubbia, Mod. Phys. Lett. A **17**, 1713 (2002).

[15] T. D. Lee and C. N. Yang, Phys. Rev. **104**, 254 (1956).

[16] S. L. Glashow, Phys. Lett. **167B**, 35 (1986).

[17] R. Foot and S. N. Gninenko, Phys. Lett. B **480**, 171 (2000).

[18] Z. Berezhiani, Int. J. Mod. Phys. A **19**, 3775 (2004).

[19] S. I. Blinnikov and M. Yu. Khlopov, Sov. J. Nucl. Phys. **36**, 472 (1982) [Yad. Phys. **36**, 809 (1982)]; Sov. Astron. J. **27**, 371 (1983) [Astron. Zh. Akad. Nauk SSSR **60**, 632 (1983)].

[20] L. Okun, hep-ph/0606202; M. Yu. Khlopov, *Cosmoparticle Physics* (World Scientific, Singapore, 1999).

[21] G. S. Atoyan *et al.*, Phys. Lett. B **220**, 317 (1989).

[22] D. Sillou, Int. J. Mod. Phys. A **19**, 3919 (2004).

[23] T. Mitsui, R. Fujimoto, Y. Ishisaki, Y. Ueda, Y. Yamazaki, S. Asai, and S. Orito, Phys. Rev. Lett. **70**, 2265 (1993).

[24] S. N. Gninenko, Phys. Lett. B **326**, 317 (1994).

[25] P. Crivelli, Int. J. Mod. Phys. A **19**, 3819 (2004).

[26] P. Crivelli, Ph.D. thesis, No. 16617, ETH Zürich, Switzerland (2006).

[27] H. Primakoff and F. T. Porter, Phys. Rev. **89**, 930 (1953); R. L. Intemann, Phys. Rev. **178**, 1543 (1969); J. Law and J. L. Campbell, Nucl. Phys. **A199**, 481 (1973); R. L. Intermann, Nucl. Phys. **A219**, 20 (1974).

[28] M. Kalimoto, T. Hyodo, and T. B. Change, J. Phys. B **23**, 589 (1990).

[29] S. Eidelman *et al.*, Phys. Lett. B **592**, 1 (2004).

[30] M. Sauter, Investigation of Background in an Experiment to Search for The Invisible Decay of Orthopositronium (Diploma work, ETHZ Switzerland, 2005).

[31] A. Badertscher *et al.*, Phys. Lett. B **542**, 29 (2002); P. Crivelli, Can. J. Phys. **80**, 1281 (2002).

[32] A. A. Prinz *et al.*, Phys. Rev. Lett. **81**, 1175 (1998).

[33] E. D. Carlson and S. L. Glashow, Phys. Lett. B **193**, 168 (1987).

[34] R. Foot, Int. J. Mod. Phys. D **13**, 2161 (2004).

[35] S. Abel, J. Jaeckel, V. V. Khoze, and A. Ringwald, hep-ph/0608248.